

Article

A Study on the Influence of Unsteady Forces on the Roll Characteristics of a Submarine during Free Ascent from Great Depth

Guo Xiang¹, Yongpeng Ou^{1,*}, Junjie Chen¹, Wei Wang¹ and Hao Wu²

¹ Department of Naval Architecture, Naval University of Engineering, Wuhan 430033, China; xiangguo1115@163.com (G.X.)

² School of Naval Architecture, Ocean and Energy Power Engineering, Wuhan University of Technology, Wuhan 430033, China; wuhao87@whut.edu.cn

* Correspondence: 19100103@nue.edu.cn

Abstract: The maximum diving depth of modern submarines has always been increasing. Although this has been useful and in some cases necessary, it usually comes with some risks. For instance, when a submarine encounters an emergency situation that requires immediate ascent from great depths, the situation becomes more dangerous, especially due to its rolling characteristics. To investigate the effect of unsteady forces during free ascent motion of submarines at great depths on submarine rolling, in this study, the SST-DDES model combined with the overset grid technique was used for the numerical simulation of a submarine free ascent. Water tank experiments for free ascent were conducted to validate the numerical approach, which confirmed the reliability of the numerical method. Following this, the CFD method was employed to conduct an initial exploratory investigation into the free ascent motion of deep-submergence submarines. The free ascent motion of submarines at great depths under five different degrees of freedom combinations was studied. The computational results indicated that submarines are more prone to roll over during free ascent at great depths. At a depth six times the length of the submarine, the maximum roll angle underwater reaches 22.8°. In addition, unsteady rolling moments, lateral forces, and yawing moments have a significant effect on submarine rolling, intensifying the tendency to roll. Furthermore, it was observed that the vertical hydrodynamic attack angle β is related to the rolling stability of the submarine, such that a moderate decrease in β is beneficial for the rolling stability. The numerical calculation method and preliminary research findings can provide theoretical support for controlling the ascent motion of real submarines.

Keywords: submarine free ascent; great depth; unsteady forces; roll; overset grid



Citation: Xiang, G.; Ou, Y.; Chen, J.; Wang, W.; Wu, H. A Study on the Influence of Unsteady Forces on the Roll Characteristics of a Submarine during Free Ascent from Great Depth. *J. Mar. Sci. Eng.* **2024**, *12*, 757. <https://doi.org/10.3390/jmse12050757>

Academic Editor: Weicheng Cui

Received: 3 April 2024

Revised: 24 April 2024

Accepted: 29 April 2024

Published: 30 April 2024



Copyright: © 2024 by the authors. Licensee MDPI, Basel, Switzerland. This article is an open access article distributed under the terms and conditions of the Creative Commons Attribution (CC BY) license (<https://creativecommons.org/licenses/by/4.0/>).

1. Introduction

With the advancement of modern scientific technology and evolving operational requirements, the maximum diving depth of submarines has been constantly increasing. For instance, according to publicly available information, the maximum operating depth (MOD) of the U.S. Seawolf-class Submarine is recorded at 610 m, approximately six times its length. In the event of an emergency surfacing requirement at great depths, submarines may face greater risks due to the vortex shedding caused by high-angle movements underwater. This phenomenon, characterized by vortex shedding in underwater motion, creates an increased risk during surfacing at significant depths, especially during the emergence phase. The occurrence of significant roll angles necessitates further investigation in order to reduce the associated risks.

Early research on the upward buoyancy of submerged objects was conducted by several scholars. For instance, Schreur [1] documented the movement of buoyant circular cylinders rising vertically (without forward speed), with and without simulated deck and

appendage geometry, albeit at low Reynolds numbers. The experiments revealed that bare cylinders exhibited unpredictable sway and yaw motions due to unsteady vortex shedding in the wake. In particular, when vertical vanes were added on top of the cylinder, roll amplitudes ranging from 30 to 150 degrees were observed. In submarine emergencies, on the other hand, significant rolling phenomena were observed during the ascent motion process for both model and actual submarines. Alternatively, Itard [2] conducted an emergency surface test with a self-propelled model by blowing off the ballast water, resulting in a roll angle of 60° during the ascent of the submarine. Furthermore, the German company Ingenieurkontor Lübeck (IKL) conducted blow tests on the forward main ballast tanks of the U206 submarine as it surfaced from a depth of 80 m, approximately twice the length of the vessel. The submarine initially navigated horizontally at a speed of 8 knots. During the surfacing process, the maximum heel angle of the submarine reached 14°, and the pitch angle reached 50° upon breaking the water surface [3]. On the other hand, Watt et al. [4] presented the motion parameters and attitude time history curves of three full-size diesel-electric submarines during emergency surfacing tests. In the surfacing test of a small submarine weighing around 1000 tons, roll angles greater than 25° were observed during submergence.

There are many factors influencing the significant rolling phenomenon during submarine surfacing. Factors such as the initial state of the submarine at surfacing, including the amount of ballast blown, the position of the ballast blown, the initial speed, and the initial posture, all have an impact. In recent years, many scholars have conducted various experimental studies, proposing different empirical models to simulate submarine surfacing. For instance, Zhang et al. [5] studied the lateral stability of submarines during surfacing through model experiments. They investigated the strong coupling effect between yaw and roll under different initial states of the submarine, such as initial speed, blown ballast longitudinal centroid, and initial rudder angle, using a combination of multiple working conditions. Their conclusions indicated that the yaw instability is a key coupling factor leading to excessive yaw angle and roll of the submarine, which has practical value for actual submarine operations. They also considered the effect of seepage holes in the experiments by adding seepage holes to the submarine model. However, the model tested was 5 m long and the water depth for the test was only 8 m, which resulted in a short surfacing time and made it difficult to analyze the influence of unsteady forces on the roll of the submarine. Alternatively, Wei et al. [6] conducted experimental research on the free surfacing of the SUBOFF submarine model and simultaneously used the Computational Fluid Dynamics (CFD) method to study the influence of different depths, launch positions, and launch amounts on the posture of the hull. However, the maximum depth in the CFD model was only about 2.5 times the length of the submarine, and the article did not address the influence of unsteady forces on the roll of the submarine. On the other hand, more attention was given to the description and analysis of posture changes during the entire process of submarine surfacing to emergence.

Compared to traditional submarine testing methods, the use of Computational Fluid Dynamics (CFD) to simulate submarine motion is more efficient, cost effective, and provides a greater level of flow detail for analyzing the physical characteristics of the submarine movement. For instance, McDonald et al. [7] employed the Reynolds-averaged Navier–Stokes (RANS) method and a six-degree-of-freedom motion solver to develop a program that studied the predictive trajectory of a full appendage SUBOFF submarine using both a volumetric force propeller model and an actual propeller model. Alternatively, Zhang et al. [8] used the RANS method to investigate the interaction between the submarine model with propellers and free-surface conditions and analyzed the impact of the free surface on the propulsion performance of the propeller. Similarly, Zaghi et al. [9] used the RANS method in conjunction with overset grids to simulate the underwater motion of a full appendage submarine, while Carrica et al. [10] analyzed the performance of the approach in predicting parameters related to the vertical zigzag maneuver of a generic submarine. Additionally, scholars such as Han et al. [11] conducted effective simulations for the movement of submarines.

Furthermore, researchers have used equations of motion with different degrees of freedom (DOF) to study the surfacing characteristics of submarines. For instance, Booth [12,13] analyzed the stability of buoyant ascent by separating the vertical and horizontal plane parameters, employing a three-degree-of-freedom analysis (3DOF analysis) based on lateral force, roll moment, and yaw moment equations using standard submarine motion equations [14]. While the main focus was on the forward motion, Booth's quasi-steady stability analysis did not consider the unsteady forces generated by vortex shedding at large angles of attack. Watt et al. [4,15,16], on the other hand, established six-degree-of-freedom motion equations based on quasi-steady coefficients, fitting the response surface models for forces in various directions within the range of angle of attack -30° to $+30^\circ$, partly addressing the instability issues observed in submarine tests. However, their analysis was limited to a specific range of angles of attack and did not consider the influence of unsteady forces.

The use of the RANS method for CFD simulation yields satisfactory results for conventional submarine scenarios with low maneuverability. However, in the case of surfacing maneuvers, which involve unconventional high-angle-of-attack motions, the prevalence of large-scale vortex separation leads to unstable unsteady forces. The use of the RANS method in this case may not be able to capture the unsteady disturbances present during submarine surfacing, potentially leading to deviations from accurate results. Although researchers such as Zhou et al. [17], Wei et al. [6,18], and Zhang et al. [19] have conducted relevant simulation studies on submarine surfacing maneuvers using the RANS method and achieved commendable results, this is probably due to the relatively shallow submersion depth, because the flow separation is not fully developed during underwater submarine motion and therefore affects the computational results less.

Research on high-angle-of-attack submarine maneuvers is relatively scarce. Liang et al. [20] conducted water tank experiments within a Circular Water Channel (CWC) equipped with a Planar Motion Mechanism (PMM) to examine the force distribution on the vertical plane of a SUBOFF submarine at an angle of attack of 60° , thereby refining the motion equations for high-angle-of-attack submarine scenarios. In aerodynamics, extensive research has been conducted on high angles of attack for slender bodies and airfoils. For instance, Binion et al. [21] discovered for the first time through missile aerodynamics studies at high angles of attack that symmetric separation vortices are stable for missiles with aspect ratios similar to submarines at angles of attack of $20\text{--}30^\circ$, while asymmetric separation vortices are stable at angles of attack of $60\text{--}70^\circ$, with instability observed at other angles.

To address vortex separation issues, an increasing number of scholars have turned to the Detached Eddy Simulation (DES) method. For instance, Sohail et al. [22] employed the SA-DES vortex separation method and introduced surface roughness to numerically simulate the asymmetric phenomena of slender bodies at high angles of attack, demonstrating good agreement with experimental data. Liu et al. [23] compared various RANS and Delayed Detached Eddy Simulation (DDES) models to simulate the static flow and forced oscillatory motions of a NACA0015 airfoil at high angles of attack, finding that the Shear Stress Transport (SST)-DDES effectively captures the vortex shedding on the leeward side of the airfoil and achieves excellent agreement with experimental unsteady aerodynamic loads, whereas RANS models performed inadequately. Wang et al. [24] utilized the DDES model to numerically simulate the unsteady flow around slender bodies at angles of attack from 0 to 180° , analyzing the results of unsteady aerodynamic forces and pulsating pressures, which exhibited good agreement with experimental data.

In summary, current research on submarine ascent motion indicates that the initial depth (H) of submarines typically falls within the range of 1–3 times the length of the submarine (L), denoted as $H/L = 1\text{--}3$. Within this depth range, the submarine's ascent velocity and duration result in an insufficient development of unsteady forces during the ascent process. Therefore, this study proposes using the MOD of the American Seawolf-class Submarine, where $H/L = 6$, as the depth for subsequent research on a submarine free ascent. Compared to the conventional $H/L = 1\text{--}3$ depth range, the $H/L = 6$ depth is considered a great depth for submarines.

To analyze the influence of horizontal unsteady disturbance forces generated on the vertical plane during the free ascent motion of a submarine at great depths, this study conducted numerical simulations of submarine free ascent using the SST $k-\omega$ two-equation turbulence model in conjunction with the DDES model and overset grid technique. In order to validate the reliability of the numerical calculation method, free ascent motion tests were conducted with a submarine model. Due to the experimental limitations, the water depth for the tests was only 1.5 times the length of the submarine. The simulation and experimental conditions were designed to match as closely as possible, encompassing the entire surfacing process of the submarine from underwater to the surface, thus enabling a fair comparison of the results. Subsequently, the factors influencing the roll motion of the submarine during free surfacing at great submersion depths were investigated. This study primarily focused on the roll behavior of the submarine during high-angle-of-attack underwater motions. Therefore, in the subsequent research, only the underwater movements of the submarine were considered by constraining different degrees of freedom of the submarine to analyze the roll characteristics during the free ascent motion.

2. Materials and Methods

2.1. Model and Coordinate System

A submarine model designed by the research team was utilized as the test model, primarily to investigate the dynamics of submarine free surfacing. The schematic diagram of the model and the definition of the hull coordinate system are illustrated in Figure 1. The submarine model consists of a main hull, casing, casing rudder, and rear “X”-shaped rudder. The model has a length (L) of 3 m and a diameter (D_L) of 0.3 m. Other key parameters of the submarine model are listed in Table 1.

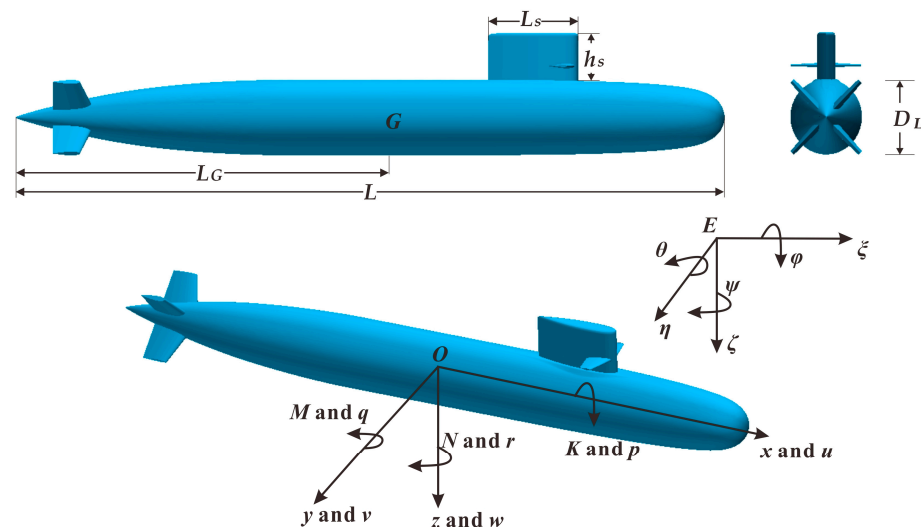


Figure 1. The submarine model and coordinate system definition.

Table 1. Main parameters of the submarine model.

Parameter	Symbol	Unit	Value
Total Length	L	m	3.0
Diameter	D_L	m	0.3
Length of Sail	L_s	m	0.32
Height of Sail	h_s	m	0.18
Stern to CG	L_G	m	1.604
Underwater Displacement	Δ	kg	170.5
Height of CB Above CG	BG	m	0.006

In this study, the coordinate system recommended by the International Towing Tank Conference (ITTC) is employed to describe the motion of the submarine [25], which is

divided into the fixed coordinate system $E-\zeta\eta\zeta$ and the body-fixed coordinate system $O-xyz$. In the body-fixed coordinate system, the origin O corresponds to the centroid of the submarine, with (u, v, w) and (p, q, r) representing the translational and rotational velocities of the submarine, respectively. Furthermore, (φ, θ, ψ) denote the Euler angles of the submarine relative to the fixed coordinate system, representing roll, pitch, and yaw angles, respectively.

2.2. Numerical Method

In the present investigation, simulation calculations were performed using the commercial fluid dynamics software STAR-CCM+ 13.02. The simulations utilized a finite volume, viscous, and incompressible unsteady DDES model. The RANS model employs the Shear Stress Transport (SST) $k-\omega$ two-equation turbulence model, which is more accurate in capturing vortex shedding compared to RANS [23]. The relative motion of the submarine model within the discrete grid was simulated using the overset grid technology, integrating the Dynamic Fluid Body Interaction (DFBI) model in STAR-CCM+ to facilitate the submarine’s underwater free ascent motion, with a time step of 0.002 s.

2.2.1. The SST Model

The DDES hybrid method is constructed based on the traditional RANS turbulence model equations. In the present work, the SST $k-\omega$ turbulence model was used, which is basically described by the following two equations:

$$\begin{cases} \frac{\partial(\rho k)}{\partial t} + \frac{\partial(\rho u_j k)}{\partial x_j} = P - \beta^* \rho \omega k + \frac{\partial}{\partial x_j} \left[(\mu + \sigma_k \mu_t) \frac{\partial k}{\partial x_j} \right] \\ \frac{\partial(\rho \omega)}{\partial t} + \frac{\partial(\rho u_j \omega)}{\partial x_j} = \frac{\rho \gamma}{\mu_t} P - \beta^* \rho \omega^2 + \frac{\partial}{\partial x_j} \left[(\mu + \sigma_\omega \mu_t) \frac{\partial \omega}{\partial x_j} \right] + 2(1 - F_1) \frac{\rho \sigma_{\omega 2}}{\omega} \cdot \frac{\partial k}{\partial x_j} \cdot \frac{\partial \omega}{\partial x_j} \end{cases} \quad (1)$$

where ρ represents the density, μ_j denotes the velocity vector, and x_j signifies the position vector. In addition, k and ω denote the turbulence kinetic energy and the specific rate of dissipation, respectively, whereas μ and μ_t are the laminar and turbulent viscosity coefficients, respectively. The form of the production term P , the function F_1 , and the values of the coefficients β^* , γ , σ_k , and $\sigma_{\omega 2}$ can be found in the literature pertinent to the SST model [26].

2.2.2. The DDES Model

The DDES model [27] reconstructs the length scale (l_{DDES}) of the DDES model by introducing a delay function, which significantly reduces the problem of modeled stress depletion (MSD) and its direct consequence, namely grid-induced separation (GIS). The DDES method is implemented in the hybrid RANS-LES-based approach in this study.

Similar to the DES method, replacing the length scale (l_{RANS}) in the turbulence model with the length scale of DDES (l_{DDES}) yields a DDES method based on the original turbulence model. The length scale (l_{DDES}) can be expressed in the following form:

$$l_{DDES} = l_{RANS} - f_d \max\{0, l_{RANS} - l_{LES}\} \quad (2)$$

The delay function (f_d) can be defined as follows:

$$f_d = 1 - \tanh[(c_d r_d)^3] \quad (3)$$

where $c_d = 8$, and the parameter r_d can be expressed as follows:

$$r_d = \frac{v + v_t}{\sqrt{u_{i,j} u_{i,j} \kappa^2 d^2}} \quad (4)$$

where v_t represents the turbulent viscosity coefficient, $u_{i,j}$ denotes the velocity gradient, $\kappa = 0.41$, and d represents the distance from the wall.

The RANS length scale of the SST turbulence model (l_{RANS}) is defined as follows:

$$l_{RANS} = \frac{k^{1/2}}{\beta^* \omega} \quad (5)$$

The length scale of the LES-based approach can be solely determined by the grid spacing:

$$l_{LES} = C_{DDES} \Delta \quad (6)$$

where Δ represents the local grid spacing. Here, Δ is taken as the maximum length of the line connecting the centers of adjacent mesh cells, i.e., $C_{DDES} = (1 - F_1)C_{DDES}^{outer} + F_1C_{DDES}^{inner}$, where $C_{DDES}^{outer} = 0.61$, $C_{DDES}^{inner} = 0.78$, and F_1 represents an internal function of the SST-based model.

According to the DDES model, it can be seen that as f_d approaches zero, the RANS calculation can be adopted, while when f_d approaches 1, it is transformed into the traditional DES method. This approach is capable of protecting the RANS calculation in the attached flow boundary layer without affecting the DES calculation in other regions.

3. Validation of Numerical Methods

The free ascent motion of the submarine was simulated using the Computational Fluid Dynamics (CFD) method. To validate the accuracy of the computational methods, free ascent experiments were conducted in a water tank. Due to the limitations of the water depth in the experiments, a water depth (H) of 4.5 m, equivalent to 1.5 times the length of the submarine, was utilized in both CFD simulations and experiments.

3.1. Free Ascent Motion CFD Simulation

The free ascent motion of the submarine was simulated using the DFBI six-degree-of-freedom motion model within the Star-CCM+ software. The entire ascent process of the submarine encompasses both underwater and surface motions, involving two phases of water and air. Multi-phase flow models were employed to address the multi-phase issue. Overset grid technology was utilized for the computational mesh, dividing the computational region into a background region and an overset grid region. After embedding the overset grid region into the background region, the overset grid region moved with the submarine.

3.1.1. Computational Domain and Boundary Conditions

Figure 2 illustrates the boundary conditions of the computational domain. In Figure 2a, the boundary conditions of the background region are depicted. The boundary surface behind the hull is set as a fluid pressure outlet, located at a distance of $4L$ from the hull. All other boundary surfaces are designated as velocity inlets. The boundary surface at the front of the hull is at a distance of $4L$ from the hull, while the left- and right-side surfaces are each at a distance of $3L$ from the hull. Also, the upper and lower boundary surfaces are located at a distance of $4L$ and $1.5L$ from the hull, respectively. The submarine is positioned at a distance of $1.5L$ from the free liquid surface. In Figure 2b, the boundary conditions of the overset grid region are all defined as overset interfaces.

3.1.2. Grids and Initial Conditions

A trim mesh was selected for the computational domain, as shown in Figure 3. The overall grids of the background region and overset grid region are depicted in Figure 3a. To facilitate the VOF model in capturing the free liquid surface, grid refinement in the vertical direction of the background region is required, with a refinement size of 8 mm. Within the overset grid region, the boundary layer of the hull consists of 5 layers, with the first layer having a y^+ value of approximately 1, and the grid size around the hull is set at 6 mm. The grids surrounding the hull undergo overall refinement with a size of 12 mm, while specific areas like the fairing and rudder receive local refinement with a size of 3 mm, as illustrated in Figure 3b. The total number of grids in the computational domain is 8.24 million, of which 3.16 million grids are in the background region and 5.08 million grids are in the overset grid region.

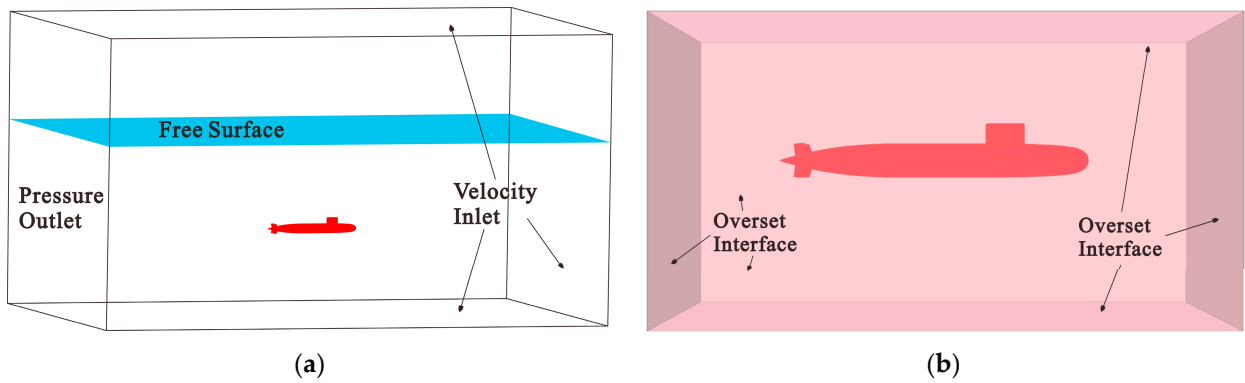


Figure 2. Computational domain and boundary conditions. (a) Background region; (b) overset grid region.

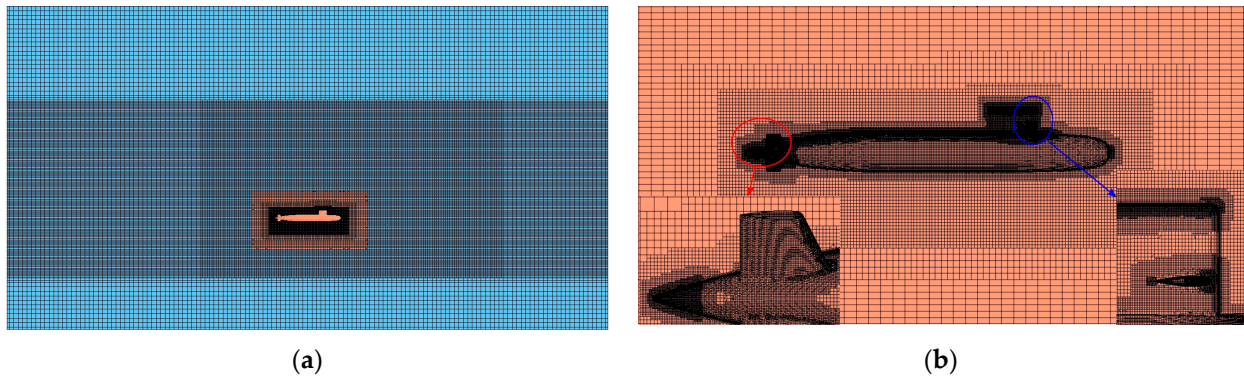


Figure 3. Computational domain grid. (a) Overall grid; (b) grid refinement around the hull.

The initial conditions for the CFD simulation of the submarine entail a launch weight of 6%, which represents a submarine gravity-to-buoyancy ratio of 94%. The center of gravity aligns with the underwater center of buoyancy in the longitudinal (x) direction of the submarine, with a height difference of only 0.006 mm, as outlined in detail in Table 2.

Table 2. Initial conditions for CFD simulation of submarine free ascent motion.

Parameter	Unit	Value
Proportion of positive buoyancy	-	6%
Positive buoyancy	kg	10.23
Center of gravity position	(m, m, m)	(0, 0, 0)
Center of buoyancy position	(m, m, m)	(0, 0, 0.006)
Depth	m	4.5
Initial posture of model	(°, °, °)	(0, 0, 0)
Initial velocity of model	(m/s, m/s, m/s)	(0, 0, 0)

3.2. Free Ascent Motion Experiment

3.2.1. Test Site and Platform

The free ascent motion test of the submarine was conducted at the outdoor water tank test site of the China Special Aircraft Research Institute. The experimental tank is 60 m long, 60 m wide, and 5.5 m deep. To facilitate the free-surface upward motion test of the submarine, a test platform was constructed within the test tank, as depicted in Figure 4. The test platform primarily consists of a platform chassis, support frame, submarine fixed platform, underwater towing carriage, lifting support, lifting watertight motor, and underwater camera system. Specific parameters of the test platform are detailed in Table 3.

Table 3. Parameters of the test platform.

Parameter	Unit	Value
Platform dimensions	m	$17 \times 4.6 \times 8.4$
Bottom guide rails	m	$13.98 \times 0.15 \times 0.16$
Platform towing carriage	m	$2.34 \times 1.12 \times 0.92$
Watertight motors	power \times number	6 kw \times 6
Underwater cameras	number	4

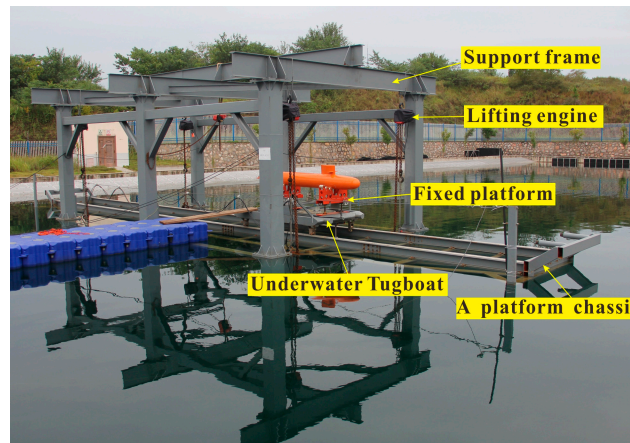


Figure 4. Photograph of the test platform.

3.2.2. Testing Equipment

To achieve the free ascent motion of the submarine, it is necessary to install the release mechanism on the submarine’s fixed platform to detach the submarine, as shown in Figure 5. Inside the submarine, an attitude sensor is installed at the center of gravity to record the roll, pitch, and yaw angles of the submarine. A depth sensor is mounted at the bottom of the submarine to come into contact with the surrounding water, measuring changes in the depth of the submarine. In addition, three-axis acceleration sensors are installed at the front, middle, and rear positions of the submarine to measure the motion state of the submarine during the upward motion. The parameters of sensors required for testing are listed in Table 4. All sensor data are collected and stored by a data acquisition system, with a data collection frequency of 100 Hz during the experiment. The entire testing system is controlled by an onshore host computer, which transmits data and control commands via optical fiber with zero buoyancy. The flowchart of the control system for the free ascent test of the submarine is shown in Figure 6.



Figure 5. Submarine release mechanism.

Table 4. Experimental sensors and main parameters.

Sensor	Measuring Range	Accuracy
Attitude sensor	Roll: $\pm 180^\circ$, Pitch: $\pm 90^\circ$, Yaw: $\pm 100^\circ$	0.05°
Depth sensor	m	1 cm
Acceleration sensor	m	0.1%

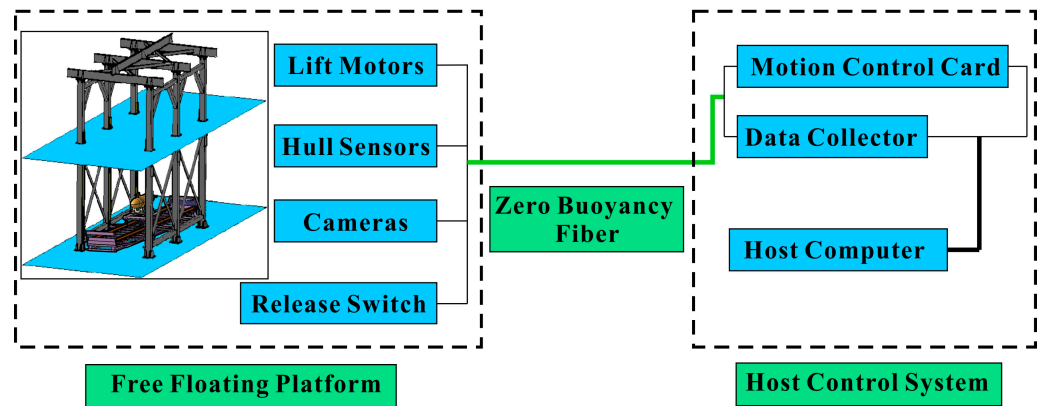


Figure 6. Experimental control system.

3.3. Comparison and Analysis of Results

To validate the accuracy of the numerical calculations, a series of experiments were conducted for the free ascent motion of the submarine in a water tank. An overview of the test details was given in the previous sections. Figure 7 presents a comparison between the time history curves of CFD and experimental free ascent motion parameters. Figure 7a–i, respectively, illustrate the longitudinal velocity u , lateral velocity v , vertical velocity w , longitudinal displacement ξ , lateral displacement η , and vertical displacement ζ , as well as the roll angle φ , pitch angle θ , and yaw angle ψ . The blue dashed lines in the figures represent the moment when the submarine model emerges from the water.

When examining the time history curves of motion velocities in three directions, particular attention is paid to the numerical simulation and experimental results of the velocities in the u and w directions. The overlap between the two sets of results is relatively high, with only minor discrepancies in peak values. From Figure 7a, it can be seen that prior to the submarine surfacing, the velocity u does not continue to increase. This phenomenon is attributed to the changes in the submarine pressure field caused by the presence of a free liquid surface. Once the submarine breaks the water surface, a rapid increase in the velocity u occurs, reaching a peak value followed by subsequent oscillations. Similarly, as seen in Figure 7c, as the submarine approaches the free liquid surface, the velocity w begins to decrease. Upon surfacing, the velocity w rapidly decreases to zero and then accelerates in the opposite direction to around -0.3 m/s, and then begins to oscillate on the water surface. In Figure 7b, three peaks are forecasted by the CFD results, whereas only two are experimentally measured. The occurrence of this phenomenon may be attributed to several factors. Firstly, it is possible that the lateral velocity v of the vessel is too low for the experimental sensors to accurately detect. Secondly, as depicted in Figure 7b, this discrepancy arises near the moment when the vessel emerges from the water, during which there is a significant alteration in vessel attitude. Consequently, there may be a slight margin of error in the sensors’ capture of v . Thirdly, when considering the overall trend, CFD generally succeeds in reflecting the variation trend of v . The presence of the free liquid surface is observed to cause changes in the submarine motion state, highlighting an aspect worthy of further investigation.

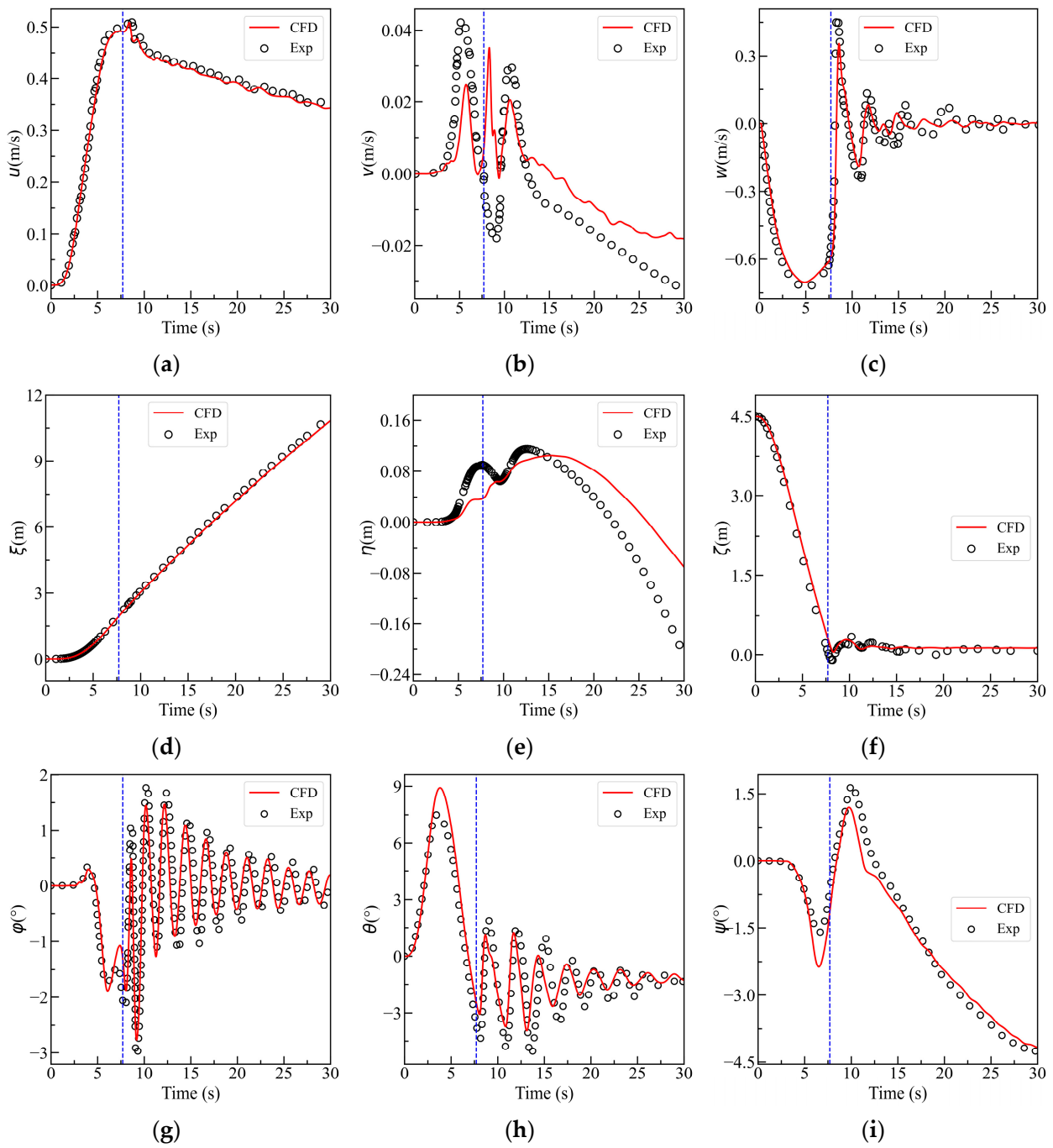


Figure 7. Comparison of time history curves of motion parameters: (a) longitudinal velocity u ; (b) lateral velocity v ; (c) vertical velocity w ; (d) longitudinal displacement ξ ; (e) lateral displacement η ; (f) vertical displacement ζ ; (g) roll angle φ ; (h) pitch angle θ ; (i) yaw angle ψ .

The displacement curves corresponding to the velocities in three directions reveal similar patterns, as illustrated in Figure 7d–f. Similarly, an overall examination of the submarine attitude angles in three directions, as shown in Figure 7g–i, indicates a basic consistency in the variation patterns between the numerical simulations and the experimental results. The roll and pitch angle motion amplitudes exhibit minor discrepancies, with good alignment in the oscillation periods on the water surface, albeit with some phase differences. Furthermore, it is observed that the surfacing of the submarine has a significant impact on the roll angle φ . Due to changes in the buoyancy state, the roll angle φ undergoes a sharp transition, posing a high risk for the submarine at this stage, potentially leading to capsizing.

Table 5 presents the characteristic values of the relevant parameters in the numerical simulation and experimental data for free surfacing motion, along with their corresponding relative errors. The errors range from 1.74% to 17.99%. It is noteworthy that for values with relatively large relative errors, the absolute errors are minimal. For instance, the absolute error for the maximum velocity v is only -0.0077 m/s, and the absolute error for the pitch angle amplitude is merely 1.419° . Therefore, in conclusion, the numerical calculation method for the free-surfacing motion of the submarine is reliable, showing a very good agreement with the experimental results. This indicates its potential for investigating the motion characteristics of deep-submergence free surfacing in future studies.

Table 5. Comparison of parameter values of free ascent motion parameters.

Parameter	Unit	CFD	Exp	Relative Error
maximum value of u	m/s	0.509	0.518	-1.74%
maximum value of v	m/s	-0.0351	-0.0428	-17.99%
maximum value of w	m/s	0.705	0.735	-4.08%
maximum value of depth	m	4.451	4.566	-2.52%
amplitude of roll angle φ	$^\circ$	-2.751	-3.053	-9.89%
amplitude of pitch angle θ	$^\circ$	-7.492	-8.911	-15.92%
amplitude of yaw angle ψ	$^\circ$	4.161	4.29	-3.01%

Figure 8 depicts the images captured at different time points during the free ascent test process of the submarine, illustrating the movements of the submarine both underwater and on the water surface. Also, Figure 9 displays images from various time points of the submarine ascent process obtained through CFD numerical simulation. It is evident that the postures predicted by the CFD calculations align well with the experimental observations.



Figure 8. The submarine state at different time points during the free ascent experiment.

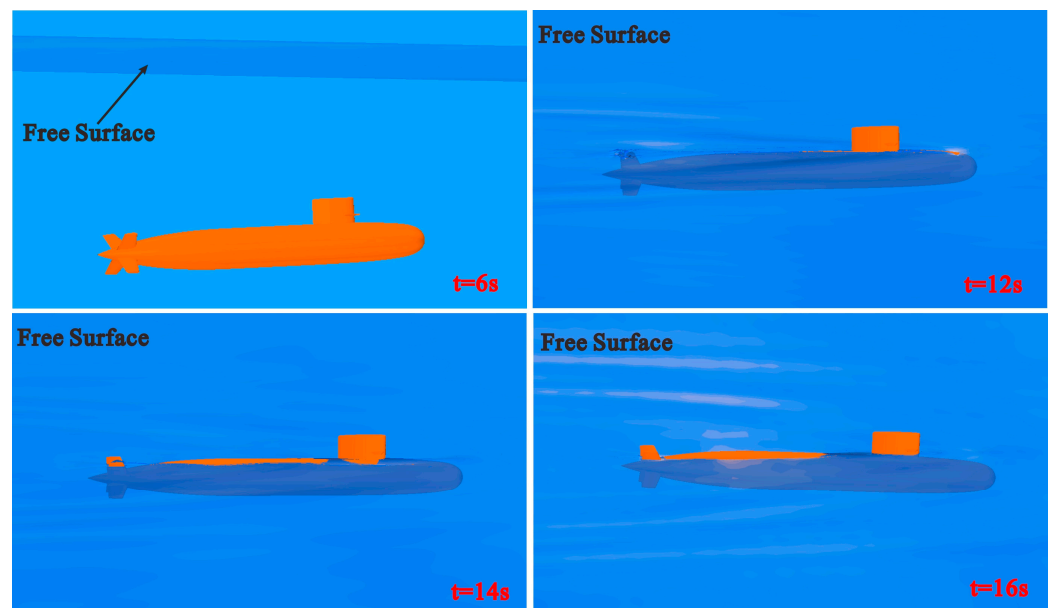


Figure 9. The submarine state during the free ascent process simulated by CFD.

4. Large Depth Ascent of the Submarine CFD Simulation

Due to limitations imposed by the experimental conditions, the water depth during the submarine free ascent test was only 4.5 m, corresponding to $H/L = 1.5$. While this made it possible to understand the patterns of submarine free ascent motion, as depicted in Figure 7c, where it is evident that the submarine's ascent velocity w had already reached its maximum before emerging from the water, the submarine's underwater motion did not fully develop before surfacing. Hence, it is imperative to conduct numerical simulations of submarine underwater motion under conditions of greater depth. In this section, a depth of $H = 18$ m, corresponding to $H/L = 6$, is selected. Considering that the submarine's ascent motion had essentially reached its maximum state at $H = 4.5$ m, indicating no fundamental difference in turbulent and unsteady characteristics between $H/L = 6$ and $H/L = 1.5$, and their Reynolds number ranges being essentially identical, the CFD methods described in the previous section are equally applicable to the $H/L = 6$ scenario.

4.1. Calculation Case Design

Based on the author's previous study [28], it has been established that when a submarine undergoes large angle-of-attack motion in the vertical plane, the unsteady disturbance forces created by the motion of the vertical plane of the submarine cannot be neglected in the horizontal plane. Therefore, to verify the effect of unsteady disturbance forces on the roll angle of an ascent submarine, simulations of a deeply submerged submarine's free ascent motion are conducted. Under the same initial conditions, the influence of unsteady disturbance forces on the roll is calculated for different degrees of freedom (DOF) during the free ascent motion of the submarine. The six DOFs for the submarine are described in Table 6, while Table 7 details specific calculation cases.

Case 1 involves releasing only the vertical motion (Z) and roll motion (R_x) DOF of the submarine to observe the effect of unsteady roll moments generated by the vertical motion on the roll. In Case 2, the lateral motion (Y) DOF within the horizontal plane is released in addition to the motions in Case 1, allowing the observation of the effect of unsteady lateral forces on the roll of the submarine. Case 3 releases four DOFs, including vertical motion (Z), lateral motion (Y), roll motion (R_x), and yaw motion (R_z), while not releasing the longitudinal motion (X) and pitch motion (R_y) DOF. This setup allows the investigation of the effect of unsteady horizontal plane forces generated solely by the vertical inflow, neglecting changes in the vertical plane angle of attack and disturbances caused by the heave motion on the roll of the submarine. Case 4, in comparison to Case 1, involves

releasing an additional longitudinal motion (X) DOF, enabling the comparison of the effect of vertical plane hydrodynamic angle of attack on the roll angle of the hull. Case 5 releases all six DOFs, providing a realistic representation of the hull roll during free-surfacing motion, reflecting the influence of unsteady disturbance forces in the horizontal plane generated by the vertical plane motion.

Table 6. Description of the six DOFs of the submarine motion.

Symbol	Description	Symbol	Description
X	Translational motion along the x -axis	R_x	Rotation around the x -axis
Y	Translational motion along the y -axis	R_y	Rotation around the y -axis
Z	Translational motion along the z -axis	R_z	Rotation around the z -axis

Table 7. Calculation case table and case purpose descriptions.

Case	DOFs	Purpose
2DOF	Z, R_x	Effect of unsteady rolling moment generated solely by vertical motion on roll
3DOF	Z, R_x, Y	Effect of unsteady rolling moment and lateral force generated solely by vertical motion on roll
4DOF	Z, R_x, Y, R_z	Effect of unsteady horizontal plane force generated solely by vertical motion on roll
5DOF	Z, R_x, Y, R_z, X	Effect of unsteady horizontal plane force generated by vertical and x -direction motion on roll
6DOF	Z, R_x, Y, R_z, X, R_y	Effect of unsteady horizontal plane force generated by vertical plane motion on roll

The initial conditions of the calculation scenarios are the same as those outlined in Section 3, with a launch angle of 6° and the position of the center of gravity unchanged. However, this simulation focuses solely on the submarine’s underwater motion and does not consider its surfacing effects. Therefore, only water is considered as the medium in the CFD calculations.

The domain size, boundary conditions, overall grid structure, and hull mesh layout are illustrated in Figure 10; the same mesh configuration is utilized for all three scenarios. Since there are no free surfaces, the vertical mesh does not require the surface refinement discussed in Section 3. The grid layout remains consistent with that described in Section 3. The total number of grid cells in the computational domain is 10.56 million, comprising 6.02 million cells in the background domain and 4.54 million cells in the overset grid domain.

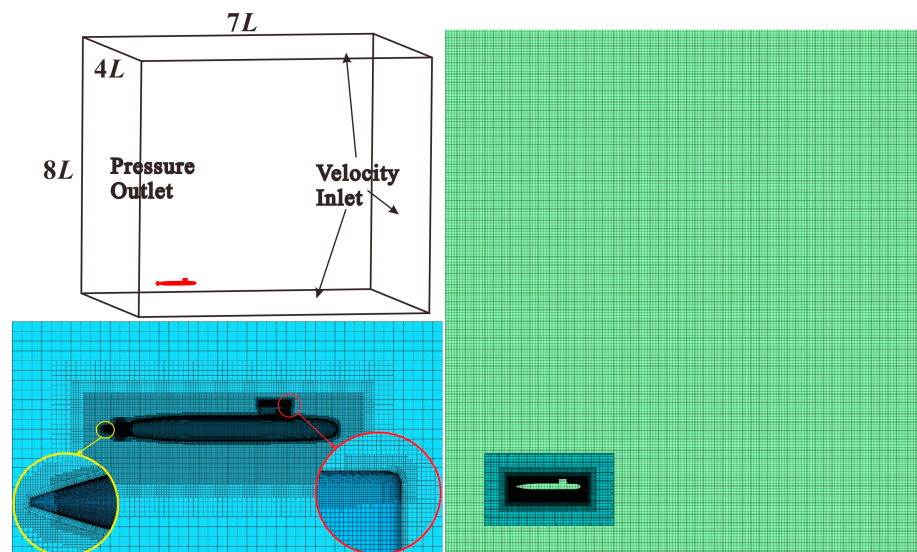


Figure 10. Computational regions and grid.

4.2. Analysis of the CFD Results

The five scenarios are divided into two groups: 2DOF, 3DOF, and 4DOF form one group, which is used to contrast the effect of the submarine’s vertical motion-induced unsteady forces in the horizontal plane on the roll angle. The other group consists of 4DOF, 5DOF, and 6DOF, and is utilized to compare the influence of submarine vertical plane motion on the unsteady forces in the horizontal plane on the roll angle.

Figure 11 presents the comparative results of the first group’s three submarine surfacing scenarios in graphical form. Figure 11a–f display the time history curves of the roll angle φ , vertical velocity w , vertical displacement ζ , lateral velocity v , lateral displacement η , and yaw angle ψ . The focus is primarily on the time history curves of the roll angle for the three scenarios. From Figure 11a, it can be observed that during the surfacing process with only two DOFs, namely Z and R_x , the roll angle amplitude is only 4.4° , indicating a certain impact of the unsteady rolling moment generated solely by the submarine vertical flow. Introducing the Y DOF, i.e., the 3DOF configuration, leads to a significant increase in roll angle fluctuation during ascent motion, with a maximum roll angle of 19.59° , highlighting a substantial influence of the unsteady lateral force generated by the submarine vertical flow on the roll angle. Further increasing the degree of freedom with R_z results in a larger maximum roll angle of 29.16° during ascent motion, demonstrating the significant impact of the unsteady pitch moment generated by the submarine vertical flow. Through a comprehensive comparison of the three scenarios, it is evident that the unsteady rolling moment produced solely by the vertical flow of the submarine, as well as the unsteady forces (f_y) and moments (M_z) in the horizontal plane, still have a considerable impact on the roll of the submarine when positioned symmetrically, and their coupled effects gradually exacerbate the roll behavior of the submarine.

Combining Figure 11b,c, it can be observed that by increasing the DOF of the submarine in the horizontal plane, the impact on the ascent speed of the submarine is minimal before the ascent of 5.3 m ($h/L = 1.76$) within 10 s. Once the surfacing speed stabilizes, the increased DOF lead to a more complex flow field that has a certain influence on the ascent speed of the submarine, resulting in slight variations in the time taken to ascent to the specified height. The ascent times for the three scenarios are 27.51 s, 28.70 s, and 29.92 s, respectively. From Figure 11d–f, it can be seen that the R_z DOF has a certain amplifying effect on the lateral velocity v of the hull, with the oscillation of the yaw angle leading to a corresponding increase in lateral displacement η . Table 8 provides a summary of the results of the relevant parameters for the first group of computational scenarios.

Table 8. Statistical analysis of the parameters for the first group of computational scenarios.

Parameter	Unit	2DOF	3DOF	4DOF
amplitude of roll angle φ	$^\circ$	4.43	19.59	29.16
maximum value of w	m/s	0.72	0.69	0.68
ascent time	s	27.51	28.70	29.92
maximum value of v	m/s	-	0.11	0.14
lateral displacement η	m	-	-0.03	-0.26
amplitude of yaw angle ψ	$^\circ$	-	-	9.20

When all the DOF in the horizontal plane of the submarine is released, the comparison of different DOF in the vertical plane impacts the horizontal forces and rolling, while the change of DOF in the vertical plane primarily affects the vertical hydrodynamic angle of attack β of the submarine, as expressed in Equation (7). Figure 12 presents a comparative plot of the calculation results for three ascent scenarios of the second group. Figure 12a–j illustrate the time history curves for roll angle φ , vertical velocity w , vertical displacement ζ , lateral velocity v , lateral displacement η , yaw angle ψ , longitudinal velocity u , longitudinal displacement ξ , pitch angle θ , and vertical hydrodynamic angle of attack β . The angle β is given by

$$\beta = \arctan(-w/u) \tag{7}$$

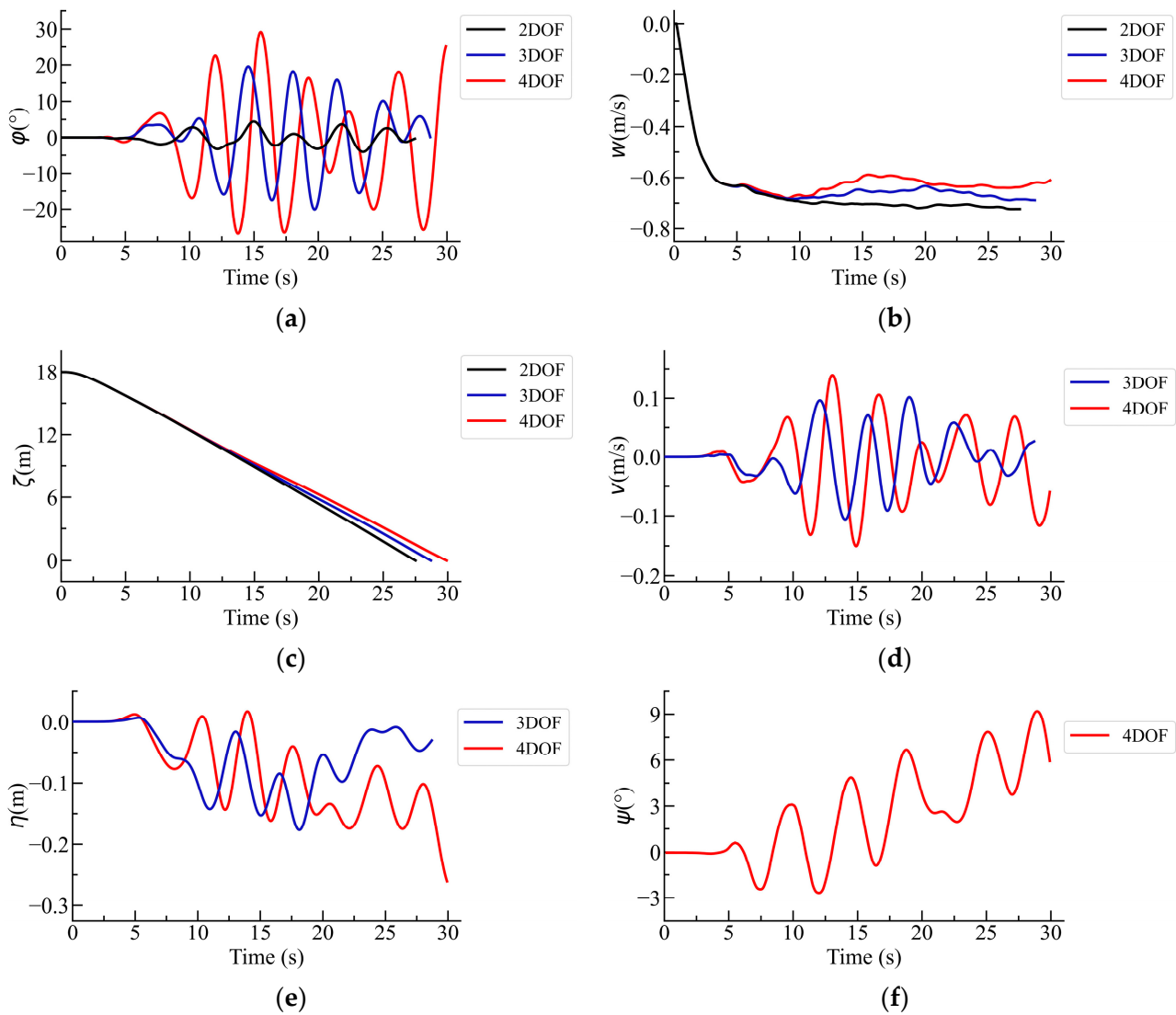


Figure 11. Results of the first group of scenarios. (a) Roll angle φ ; (b) vertical velocity w ; (c) vertical displacement ζ ; (d) lateral velocity v ; (e) lateral displacement η ; (f) yaw angle ψ .

Firstly, by observing the time history curves of roll angle for the three scenarios, it can be seen from Figure 12a that in the roll angle time history curve, when the X DOF of the submarine is released, i.e., in the 5DOF case, the fluctuation in the rolling time history curve is significantly reduced compared to the 4DOF condition, with a maximum roll angle amplitude of 16.7° . This indicates that the presence of longitudinal velocity u in the submarine favors its rolling stability. Furthermore, it can be inferred that by decreasing the vertical hydrodynamic angle of attack β of the submarine, the roll angle of the submarine can be improved. When all six DOFs of the submarine are released, the rolling time history curve fluctuates between the 4DOF and 5DOF case, with a maximum roll angle amplitude of 22.8° . Combining this with the pitch angle θ from Figure 12i and the vertical hydrodynamic angle of attack β time history curve from Figure 12j, the hull transitions to a “bow-down” state as the speed w reaches a certain value, leading to a reduction in hull speed u . This causes the angle β of the 6DOF case to be greater than that of the 5DOF after $t = 11.5$ s, which negatively affects the roll stability of the hull compared to the 5DOF case. In conclusion, during the ascent process, the vertical hydrodynamic angle of attack β of the submarine is related to its rolling stability, and reducing β appropriately is beneficial for enhancing rolling stability.

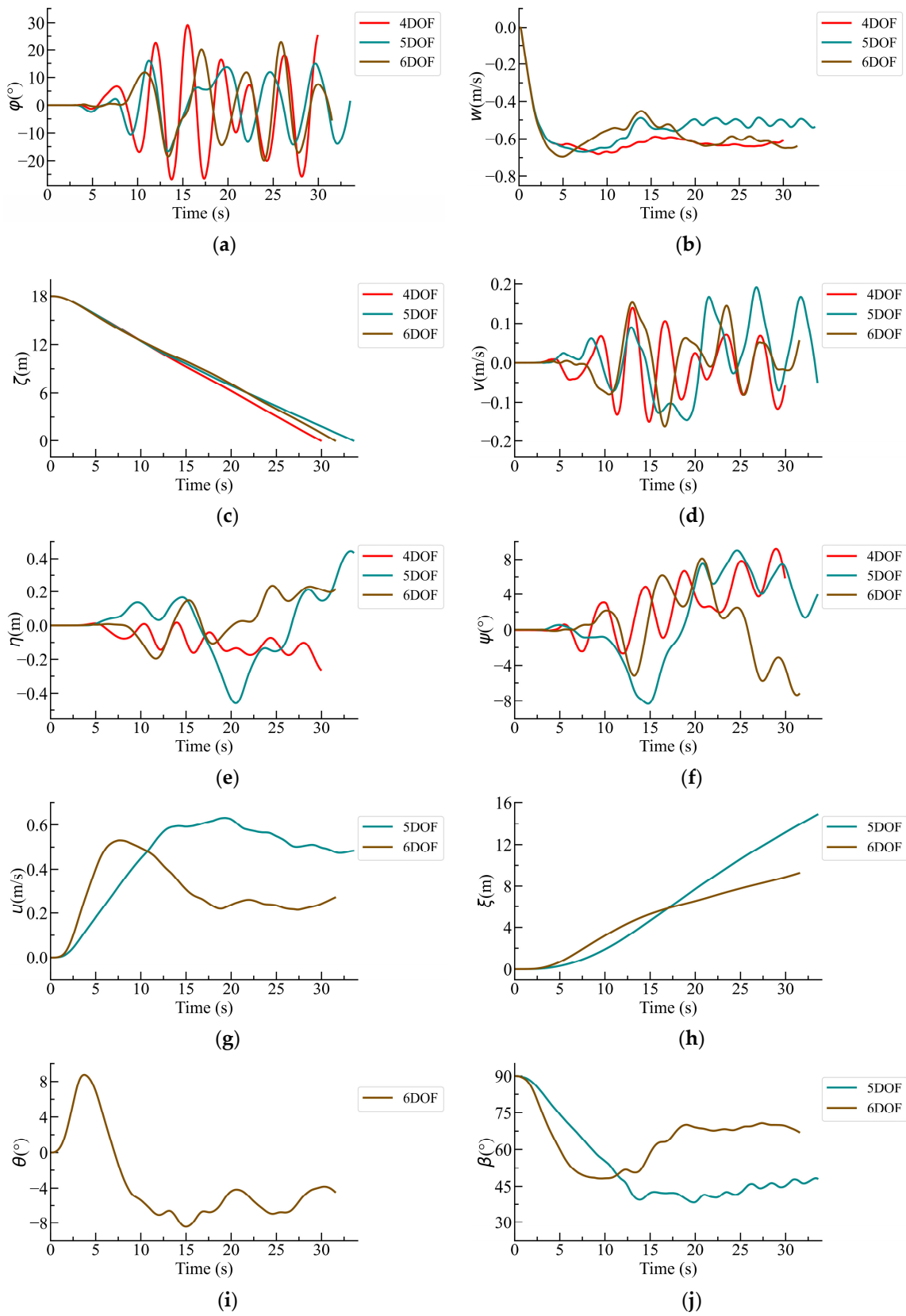


Figure 12. Results of the second group of scenarios. (a) Roll angle φ ; (b) vertical velocity w ; (c) vertical displacement ζ ; (d) lateral velocity v ; (e) lateral displacement η ; (f) yaw angle ψ ; (g) longitudinal velocity u ; (h) longitudinal displacement ξ ; (i) pitch angle θ ; (j) vertical plane hydrodynamic angle of attack β .

Combining Figure 12b for speed w and Figure 12c for displacement ζ , it can be observed that as the surfacing progresses in the 5DOF case, the deceleration of speed w is most pronounced among the three scenarios. In the 6DOF case, the speed w exhibits the greatest fluctuation, indicating that the variations in the pitch angle of the submarine affect the surfacing speed w , consequently impacting the surfacing time of the hull. Observing Figure 12d for speed v and Figure 12e for displacement η , the presence of degrees of freedom X and R_y has minimal impact on the magnitude of the lateral speed v but exacerbates its fluctuations. Similarly, variations in the yaw angle also intensify its fluctuations with minimal impact on its magnitude. By observing Figure 12g for speed u and Figure 12h for displacement ζ , it is evident that the changes in the pitch angle θ significantly affect the hull speed u , resulting in a decrease of 0.1 m/s, or a reduction of 16.1%, in the speed u of the 6DOF case compared to the 5DOF case. The fluctuation range increases from 0.157 m/s in the 5DOF case to 0.316 m/s in the 6DOF case. When the hull ascent reaches 18 m, the longitudinal displacement decreases by 5.6 m. Table 9 summarizes the results of the relevant parameters for the second group of computational scenarios.

Table 9. Statistical analysis of the parameters for the second group of computational scenarios.

Parameter	Unit	2DOF	3DOF	4DOF
amplitude of roll angle φ	°	29.16	16.96	22.65
maximum value of w	m/s	0.68	0.69	0.67
ascent time	s	29.92	33.52	31.49
maximum value of v	m/s	0.14	0.19	0.16
lateral displacement η	m	−0.26	0.43	0.21
amplitude of yaw angle ψ	°	9.20	9.03	8.12
maximum value of u	m/s	-	0.63	0.53
longitudinal displacement ζ	m	-	14.87	9.29
amplitude of pitch angle θ	°	-	-	8.76
minimum value of β	°	-	38.31	48.12

Figure 13 depicts the vortex quantities around the submarine hull at various instants during the 6DOF free ascent motion. In the early stages of motion, when the submarine speed w is low, the vortex quantities around the hull are not prominent, with only a small number of vortices present near the casing and rudder. The hull is in a “bow-up” posture. As the speed w increases, the flow field around the hull gradually becomes more intricate, with significant growth in vortex quantities. Moreover, the hull posture transitions from “bow up” to “bow down,” which is accompanied by asymmetry in the left and right vortices of the hull. Consequently, the hull motion becomes progressively intricate.

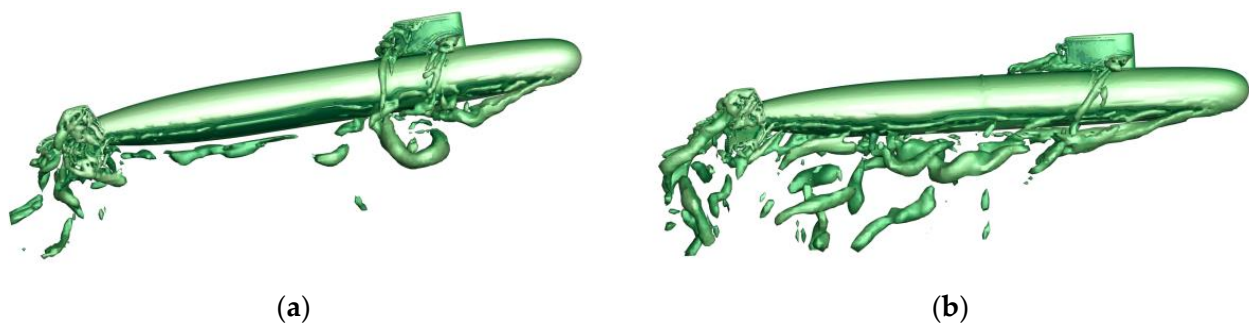


Figure 13. Cont.

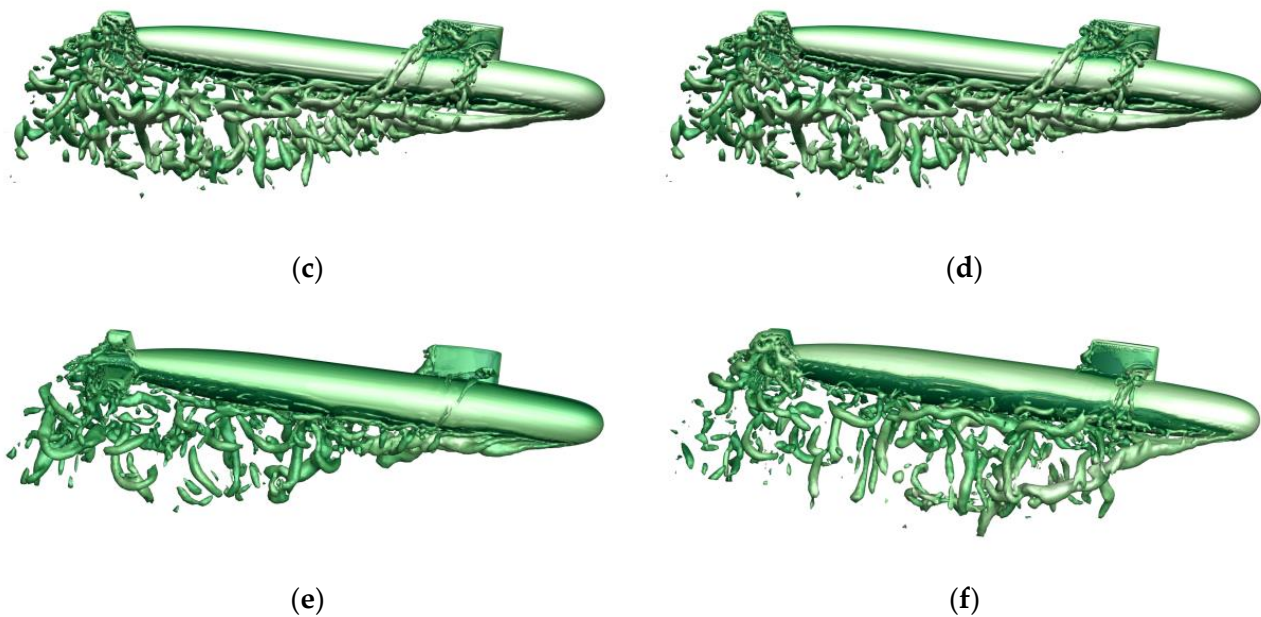


Figure 13. Vortex quantities and attitude diagram of the submarine at different instants during deep free ascent motion. (a) $t = 4$ s; (b) $t = 6$ s; (c) $t = 10$ s; (d) $t = 12$ s; (e) $t = 14$ s; (f) $t = 16$ s.

5. Discussion and Conclusions

The preliminary exploration of submarine deep free ascent motion is conducted in this study using a CFD approach employing the SST-DDES model combined with overset grid techniques. Firstly, to validate the reliability of the numerical method, a free ascent experiment of a submarine model was conducted. Due to the limitations of the test conditions, the water depth for the experiment was only 1.5 times the length of the submarine. The numerical calculations were consistent with the experimental conditions, covering the entire ascent process of the submarine underwater and at the water surface, and were compared and verified against the experimental results. Subsequently, the numerical simulation of the free ascent motion of the submarine was performed at a depth of 6 times the length of the submarine. By constraining the different combinations of degrees of freedom of submarine motion, the five calculation scenarios were divided into two groups to analyze the effect of unsteady disturbance forces on the roll motion during the free ascent of the submarine. The main preliminary conclusions are as follows:

- (1) The simulation of submarine free ascent motion using the SST-DDES model with overset network technology has been proven to be feasible and reliable. A comparison between the CFD calculations and the experimental results of the submarine free ascent model reveals a good agreement in the time history curves of velocity, displacement, and attitude angles in different directions. The majority of the errors in the amplitude of motion parameters are within 5%, with only the relative errors of the lateral velocity, roll angle, and pitch angle exceeding 10%. However, their absolute errors remain minimal.
- (2) At great depth, the submarine is more prone to significant rolling during free ascent. Under such conditions, the ascent motion of the hull is fully developed, leading to unsteady rolling moments, lateral velocity, and yawing moments generated by the vertical plane motion of the submarine, resulting in increased rolling of the hull. When starting from the same initial state, the maximum roll angle of the hull underwater is 1.9° at a depth of 1.5 times the submarine's length, while it reaches 22.8° when ascending at a depth of 6 times its length.
- (3) When considering only the vertical degree of freedom in the motion of the submarine, a comparison of different conditions of horizontal plane freedom reveals that the unsteady roll moment, lateral force, and yawing moment induced solely by the vertical

flow around the submarine have a significant impact on the roll of the submarine. Moreover, the combined effect of these three factors gradually exacerbates the roll of the submarine.

- (4) By altering the conditions of the submarine's vertical plane freedom, it has been observed that the hydrodynamic angle of attack β of the vertical plane during ascent is related to the rolling stability of the submarine. Appropriate reduction of β is beneficial for the rolling stability of the submarine.
- (5) The free ascent motion of a submarine involves complex and highly nonlinear dynamics, and the unsteady forces on the submarine cannot be ignored. This study has only conducted preliminary exploratory research using the CFD method. Further physical investigations will be required in subsequent research. Additionally, this study provides preliminary theoretical support for controlling the free ascent motion of actual submarines and lays the groundwork for future research on the prediction of submarine unsteady forces.

Author Contributions: Conceptualization, G.X. and Y.O.; methodology, G.X. and J.C.; validation, H.W., W.W. and Y.O.; writing—original draft preparation, G.X.; writing—review and editing, Y.O. and H.W.; supervision, W.W.; project administration, Y.O.; funding acquisition, Y.O. All authors have read and agreed to the published version of the manuscript.

Funding: This work was supported by the Pre-Research on Equipment (Shared Technology) of China under Grant 41407020602.

Institutional Review Board Statement: Not applicable.

Informed Consent Statement: Not applicable.

Data Availability Statement: The data presented in this study are available on request from the corresponding author. The data are not publicly available due to privacy or ethical restrictions.

Conflicts of Interest: The authors declare no conflicts of interest.

References

1. Schreur, B.G.J.W. The Motion of Buoyant Bodies. Ph.D. Thesis, Trinity College, Cambridge, UK, 1990.
2. Itard, X. Recovery procedure in case of flooding. In Proceedings of the Warship-International Symposium then Conference, Brisbane, Australia, 22–25 August 1999.
3. Lv, B.; Huang, B.; Peng, L. Review on high-pressure air blowing the submarine main ballast tanks. *Ship Sci. Technol.* **1992**, *42*, 40–67.
4. Watt, G.D.; Bohlmann, H.J. Submarine rising stability: Quasi-steady theory and unsteady effects. In Proceedings of the 25th Symposium on Naval Hydrodynamics, St. John, NL, Canada, 8–13 August 2004.
5. Zhang, S.; Li, H.; Pang, Y.; Chen, Q.; Yan, P. Experimental investigation on roll stability of blunt-nose submarine in buoyantly rising maneuvers. *Appl. Ocean. Res.* **2018**, *81*, 34–46. [[CrossRef](#)]
6. Wei, K.; Gao, X.; Luo, P.; Li, Y. Research on the buoyancy motion of a submarine in calm water. *Ships Offshore Struct.* **2023**, *18*, 302–314. [[CrossRef](#)]
7. McDonald, H.; Whitfield, D. Self-propelled maneuvering underwater vehicles. In *Proceedings of the 21st Symposium on Naval Hydrodynamics*; National Academy Press: Washington DC, USA, 1997; pp. 478–489.
8. Zhang, N.; Zhang, S.-l. Numerical simulation of hull/propeller interaction of submarine in submergence and near surface conditions. *J. Hydrodyn.* **2014**, *26*, 50–56. [[CrossRef](#)]
9. Zaghi, S.; Di Mascio, A.; Broglia, R.; Muscari, R. Application of dynamic overlapping grids to the simulation of the flow around a fully- appended submarine. *Math. Comput. Simul.* **2015**, *116*, 75–88. [[CrossRef](#)]
10. Carrica, P.; Kim, Y.; Martin, J. Vertical zigzag maneuver of a generic submarine. *Ocean. Eng.* **2021**, *219*, 108386. [[CrossRef](#)]
11. Han, K.; Cheng, X.; Liu, Z.; Huang, C.; Chang, H.; Yao, J.; Tan, K. Six-DOF CFD simulations of underwater vehicle operating underwater turning maneuvers. *J. Mar. Sci. Eng.* **2021**, *9*, 1451. [[CrossRef](#)]
12. Booth, T.B. Stability of buoyant underwater vehicles: Part I. Predominantly forward motion. *Int. Shipbuild. Prog.* **1977**, *24*, 297–305. [[CrossRef](#)]
13. Booth, T.B. Stability of buoyant underwater vehicles: Part II. Near vertical ascent. *Int. Shipbuild. Prog.* **1977**, *24*, 346–352. [[CrossRef](#)]
14. Gertier, M.; Hagen, G.R. *Standard Equations of Motion for Submarine Simulation*; Naval Ship Research and Development Center Bethesda: Rockville, MD, USA, 1967.
15. Watt, G.D.; Hooft, J. A Quasi-Steady Evaluation of Submarine Rising Stability: The Stability Limit. In Proceedings of the RTO-AVT Symposium on Advanced Flow Management, Loen, Norway, 7–11 May 2001.

16. Watt, G.D. *Modelling and Simulating Unsteady Six Degrees-of-Freedom Submarine Rising Maneuvers*; Defence R&D Canada-Atlantic: Dartmouth, NS, Canada, 2007.
17. Zhou, G.; Ou, Y.; Gao, X.; Liu, R. Overset Simulations of Submarine's Emergency Surfacing Maneuvering in Calm Water and Regular Waves. *J. Ship Mech.* **2018**, *22*, 1471–1482.
18. Wei, K.; Gao, X.; Liu, D.; Wei, F.; Luo, P. Research on the submarine floating movement in waves involving the water holes. *Ocean. Eng.* **2023**, *272*, 111326. [[CrossRef](#)]
19. Zhang, S.; Li, H.; Zhang, T.; Pang, Y.; Chen, Q. Numerical simulation study on the effects of course keeping on the roll stability of submarine emergency rising. *Appl. Sci.* **2019**, *9*, 3285. [[CrossRef](#)]
20. Liang, X.; Ma, N.; Liu, H.; Gu, X. Experimental study on the maneuvering derivatives of a half-scale SUBOFF model in the vertical plane. *Ocean. Eng.* **2021**, *233*, 109052. [[CrossRef](#)]
21. Binion, T.; Stanewsky, E. Observed Reynolds Number Effects: Low Aspect Ratio Wings and Bodies. In *Reynolds Number Effects in Transonic Flow*; AGARD-AG-303; Specialised Printing Services Limited: Loughton, UK, 1988.
22. Sohail, M.; Chao, Y.; Ullah, R.; Yamin, M. Computational challenges in high angle of attack flow. *World Acad. Sci. Eng. Technol.* **2011**, *80*, 1148–1155.
23. Liu, Z.; Yang, Y.; Zhou, W.; Gong, A. Study of Unsteady Separation Flow Around Airfoil at High Angle of Attack Using Hybrid RANS-LES Method. *Acta Aeronaut. Astronaut. Sin.* **2014**, *35*, 372–380.
24. Wang, F.; Liu, J.; Qin, H.; Song, Y.; Chen, L.; Hu, J. Unsteady aerodynamic characteristics of slender body at extra-wide angle-of-attack range. *Aerosp. Sci. Technol.* **2021**, *110*, 106477. [[CrossRef](#)]
25. SNAME. *Nomenclature for Treating the Motion of a Submerged Body through a Fluid*; Technical Research Bulletin; The Society of Naval Architects and Marine Engineers: New York, NY, USA, 1950; pp. 1–5.
26. Menter, F.R. Two-Equation Eddy-Viscosity Transport Turbulence Model for Engineering Applications. *AIAA J.* **1994**, *32*, 1598–1605. [[CrossRef](#)]
27. Spalart, P.R.; Deck, S.; Shur, M.L.; Squires, K.D.; Strelets, M.K.; Travin, A. A New Version of Detached-eddy Simulation, Resistant to Ambiguous Grid Densities. *Theor. Comput. Fluid Dyn.* **2006**, *20*, 181–195. [[CrossRef](#)]
28. Xiang, G.; Ou, Y.; Chen, J.; Wang, W.; Wu, H. Numerical Study on the Flow Characteristics of High Attack Angle around the Submarine's Vertical Plane. *Appl. Sci.* **2024**, *14*, 395. [[CrossRef](#)]

Disclaimer/Publisher's Note: The statements, opinions and data contained in all publications are solely those of the individual author(s) and contributor(s) and not of MDPI and/or the editor(s). MDPI and/or the editor(s) disclaim responsibility for any injury to people or property resulting from any ideas, methods, instructions or products referred to in the content.